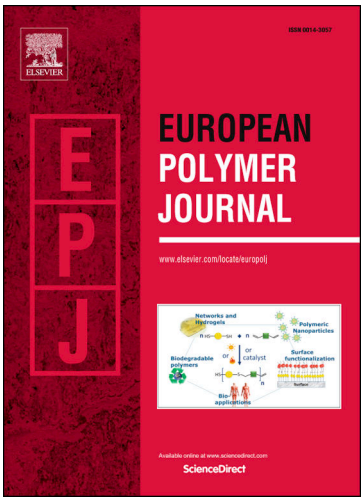

Journal Pre-proofs

A COMPREHENSIVE EVALUATION OF FLEXIBLE FDM/FFF 3D PRINTING FILAMENT AS A POTENTIAL MATERIAL IN MEDICAL APPLICATION

Agnieszka Haryńska, Iga Carayon, Paulina Kosmela, Kamil Szeliski, Marcin Łapiński, Marta Pokrywczyńska, Justyna Kucińska-Lipka, Helena Janik

PII: S0014-3057(20)31672-4
DOI: https://doi.org/10.1016/j.eurpolymj.2020.109958
Reference: EPJ 109958

To appear in: *European Polymer Journal*

Received Date: 9 July 2020
Revised Date: 11 August 2020
Accepted Date: 16 August 2020

Please cite this article as: Haryńska, A., Carayon, I., Kosmela, P., Szeliski, K., Łapiński, M., Pokrywczyńska, M., Kucińska-Lipka, J., Janik, H., A COMPREHENSIVE EVALUATION OF FLEXIBLE FDM/FFF 3D PRINTING FILAMENT AS A POTENTIAL MATERIAL IN MEDICAL APPLICATION, *European Polymer Journal* (2020), doi: https://doi.org/10.1016/j.eurpolymj.2020.109958

A COMPREHENSIVE EVALUATION OF FLEXIBLE FDM/FFF 3D PRINTING FILAMENT AS A POTENTIAL MATERIAL IN MEDICAL APPLICATION

Agnieszka Haryńska[1,*], Iga Carayon[1], Paulina Kosmela[1], Kamil Szeliski[3], Marcin Łapiński[2], Marta Pokrywczyńska[3], Justyna Kucińska-Lipka[1], Helena Janik[1]

[1] Department of Polymers Technology, Faculty of Chemistry, Gdansk University of Technology (GUT), Narutowicza Street 11/12, 80-233 Gdansk, Poland

[2] Department of Solid State Physics, Faculty of Applied Physics and Mathematics, Gdansk University of Technology (GUT), Narutowicza Street 11/12, 80-233 Gdansk, Poland

[3] Department of Regenerative Medicine, Cell and Tissue Bank, Nicolaus Copernicus University, Collegium Medicum, M.Sklodowskiej-Curie 9, 85-094 Bydgoszcz, Poland

* Correspondence: agnieszka.harynska@pg.edu.pl (AH)

ABSTRACT

The use of FDM/FFF in 3D printing for medical sciences is becoming common. This is due to the high availability and decent price of both 3D printers and filaments useful for FDM/FFF. Currently, researchers' attention is focused mainly on the study of medical filaments based on PLA, PCL or their modifications. This contributes to insufficient diversity of medical-grade filaments on the market. Moreover, due to the lack of specified standards for filaments testing, manufacturers often provide merely the characteristics of the raw materials, which were used for filaments fabrication. This lack of comprehensive data can be problematic when considered as a filament of medical 3DP application. As a consequence of this overview, we have performed a comprehensive evaluation of a flexible medical-grade filament for FDM/FFF 3DP - Bioflex® (Filoalfa). We have performed complex characterization of Bioflex® through a variety of methods and techniques including spectroscopic analysis (FTIR, Raman), dynamic mechanical analysis (DMA), thermal properties (DSC, TGA), rheological characteristic (MFR). In the next step, Bioflex® was used for 3DP and obtained printouts were utilized to characterize the material behaviour after 3D printing process. The mechanical analysis allowed to estimate how the material strength decreases after the printing process according to the values given in the technical data sheet of Bioflex®. The contact angle measurements determined wettability of the Bioflex® printouts. Performed series of in vitro studies were carried out to assess its potential as constructs having direct contact with the human body as implantable structures. In conclusion, 3D printing process did not affect the printouts biocompatibility (ISO 10993:5). Accelerated degradation studies indicated elevated hydrolysis resistance of printed samples. In turn, performed incubation in simulated body fluid (SBF) solution, revealed carbonated hydroxyapatite (HAp) deposition on printouts surface indicating their bioactive properties. Thus, studied filament Bioflex® seems to be a suitable candidate for further development of FDM/FFF 3DP structures for advanced biological and medical application.

KEYWORDS: Material characterization, Fused Deposition Modelling, 3D printing, Medical-grade filament, Bioactivity, Simulated body fluid (SBF)

1. Introduction

Biopolymers, both natural and synthetic, have been known in medicine for centuries. Due to the simplicity of their formation, biocompatible or biostable nature and a wide range of the properties that can be adapted to the desired needs, they constantly attract the interest of scientists and the medical industry [1]. Progress in the field of polymers is, among others, associated with the research on modern and advanced methods of their processing technologies. Although the basic thermoplastics forming methods such as extrusion, thermoforming or injection moulding are still used in the medical industry, improved processes for the formation of personalized complex structures in a time-saving and efficient way are desirable. These methods include additive manufacturing technologies AM (so-called 3D printing). The use of AM technologies created wide opportunities especially in the field of personalized medicine and drug delivery [2–4]. Fused deposition modelling (FDM, Stratasys, USA) / Fused Filament Formation (FFF, non-trademark) are 3DP technologies that form objects by extrusion of thermoplastic-based material supplied in the form of the filament. Here, molten material is deposited layer by layer on the build table following the loaded computer data. The FDM/FFF technologies belong to the group of extrusion-based 3D printers. They have gained particular attention in medicine, pharmaceutical industry as well as various branches of science due to the high accessibility, relatively low production or equipment costs [5]. Thereby, advanced products such as anatomical models and surgical training systems [6–8], drug delivery systems [9–11], dialysis catheters [12,13], customized laboratory equipment [14,15] or tissue engineering scaffolds [16–18] are successfully formed using FDM/FFF 3D printers. Since the selection of an appropriate material for the production of medical prototypes (objects that do not interact with biological matter) is not an issue, the 3DP of objects having permanent or short-term contact with tissues should utilize medical-grade materials. Considering filament market, the number of the certified, medical-grade materials is constantly increasing, however, the choice is still limited. Some of them are briefly described in Table 1.

Table 1 Review of selected commercial medical-grade filaments for FDM/FFF 3D printing. Presented data are taken from TDS available on the manufacturers' websites.

Trade name (company)	Bioflex® (Filoalfa)	Arnitel® ID 2045 (DSM)	FibreTuff® II (IPM)	guidel!ne® (taulman3D)
Chemical family/product description	TPC (thermoplastic copolyester elastomer)	TPC (thermoplastic copolyester elastomer)	PMC (composite based on polyamide, polyolefin and cellulose fibres)	PETG based (glycol-modified polyethene terephthalate)

Mechanical properties	Tensile modulus (MPa)	35 (ASTM D790)	29 / 29* (ISO 527)	850 (ISO 527)	1940 (ASTM D412)
	Tensile strength (MPa)	16 (ASTM D638)	8 / 7.6* (ISO 527)	23 (ISO 527)	47 (ASTM D412)
	Elongation at break (%)	800 (ASTM D638)	350 / 390* (ISO 527)	4 (ISO 527)	5.9 (ASTM D412)
	Hardness	27 Sh D (ASTM D2240)	34 Sh D (ISO 868)	-	-
Thermal properties	Melting point (°C)	185 (ASTM D3417)	158 (ISO 11357)	-	220
	Glass transition temperature (°C)	–70	–35 (ISO 11357)	-	77
Biological evaluation of medical devices		USP Class VI ISO 10993-4/5/10	USP Class VI ISO 10993-5/10	USP Class VI	USP Class VI ISO 10993-3/4/5/6/10/11 ISO 11607-1 DMF (type III)

- tests conducted on printed specimens. * - infill raster orientation 0/90° and ±45°, respectively.

In general, filament manufacturers provide comprehensive material characteristics, but most of the data concerns to a raw material from which filament was formed. So far, there are no specified requirements or standards describing how the material data related to filament should be presented. This leads to inconsistencies in the developed research with their use. FDM/FFF 3DP is based on a combination of high-temperature extrusion process and application of mechanical stress. Thus, we can expect changes in polymer properties and the general characteristic is no longer comparable to data provided by a manufacturer [19]. Moreover, this issue is becoming even more complex when factors affecting the FDM/FFF 3D printout properties are taken under consideration. The list of factors affecting the quality and mechanical properties of the FDM/FFF printouts has been reliably presented by Goh et al. [20]. They include the print orientation on build table, temperature parameters, print speed, extrusion ratio, nozzle diameter, infill properties, layer thickness, flow rate or cooling factors.

The extensive material characterization seems particularly important when we consider using FDM/FFF printed structures for medical purposes [21]. The characterization should include biological and degradation tests. Besides *in vitro* cytotoxicity, cell adhesion, long and short-term degradation studies [21–23], the incubation in simulated body fluid (SBF) is desirable since it is a very effective method to assess material bioactivity in terms of apatite formation ability [24]. It is worth noting, that SBF solution is characterized by ion concentration nearly the same to those of human blood plasma. Most of the bone-bonding materials subjected to SBF solution form on their surface a mineral structure (apatite) by which they bond and adapt to living bone tissues [25].

Material data provided by the Bioflex® manufacturer refer to the properties of the raw material used for its fabrication, hence it seems reasonable to extend the product characteristic with the properties of the filament and printouts obtained from it. Therefore, we conducted a series of studies to assess whether and how the FFF 3D printing process affects filament and printout properties compared to the source material. For this purpose, we analyzed a chemical structure and determined thermal, thermomechanical, mechanical, rheological and surface properties. Bioflex® filament is marked as suitable for medical certifications (USP Class VI and ISO 10993-4/5/10), thus we carried out preliminary tests to evaluate its potential application for structures, which can interact with a human body. Printouts in the form of porous meshes were subjected to cytotoxicity test, short-term degradation studies as well as incubation in simulated body fluid (SBF) for *in vitro* biomineralization evaluation. Cytotoxicity test was carried out with the use of CCl163 cell line according to requirements given by ISO 10993-5 standard. The degradation process was monitored via FTIR spectroscopy and mass change measurement. The apatite deposition on the printout's surface after SBF incubation was examined by SEM supplemented by EDS and Raman spectroscopy.

2. Material and methods

2.1. Material

Bioflex® filament was purchased from Filoalfa, Italy. It is a flexible fibre marked as a copolyester with USP VI class and ISO 10993-4/5/10 medical certifications. Filament has a milky white colour and a diameter of 1.75 mm. Table 1 shows the extended product characteristics. Recommended print settings are as follows, extruder temperature 210-230°C, bed temperature 0-70°C and printing speed 40-60 mm s^{-1}.

2.2. 3D printer and test sample preparation

Inventor I series FFF 3D printer (FlashForge, China) in conjunction with FlashPrint slicer (4.2.0 version, FlashForge, China) was used to form test printouts. The following basic print settings were maintained: extruder temperature 220°C, bed temperature 50°C, printing speed 20-40 mm s^{-1} and nozzle diameter 0.4 mm. For detailed information on test samples design and printing parameters please see Supplementary data. The filament was examined as received.

2.3. Filament characterization methods

2.3.1. Spectroscopic studies

Spectroscopic studies were carried out to examine the chemical functional groups of Bioflex® filament to evaluate the impact of the printing process on its stability. Thus, the filament and printouts were investigated. Attenuated total reflectance (ATR) FTIR analysis was conducted with a Nicolet 8700 spectrometer (Thermo Fisher Scientific, Waltham, USA) at spectral range of 4000-500 cm^{-1} (64 scans, resolution 4 cm^{-1}) under room temperature. Raman spectra were collected using a confocal micro-Raman system (InVia, Renishaw, UK) at randomly selected locations (50x magnification) with a green laser (514 nm) operating at 50% of its total power (50 mW).

2.3.2. Thermal properties

To determine thermal behaviour and stability of the filament and printouts, differential scanning calorimetry (DSC) and thermogravimetry (TG) were applied. DSC measurements were performed using a Netzsch 204F1 Phoenix apparatus (Netzsch, Germany) under nitrogen atmosphere (flow rate 20 mm min^{-1}). Approximately 5 mg samples were placed in aluminium crucibles. Heating/cooling cycle

was performed as follows; Initially, the sample was heated to 250°C. Once the temperature was reached, it was cooled to –80°C and reheated to 250°C. The heating/colling rate was 10°C min^{-1}. In turn, thermogravimetric analysis was carried out using a Netzsch TG 209 instrument (Netzsch, Germany). Samples of ~5 mg were studied at a heating rate of 10°C min^{-1} in the temperature range from 35°C to 700°C under nitrogen atmosphere.

2.3.3. Dynamic mechanical analysis (DMA)

The dynamic mechanical test was performed using DMA Q800 analyzer (TA Instruments, USA). Printouts having dimensions of 40 × 10 × 2 mm were measured in the single cantilever bending mode with 1 Hz frequency of an oscillatory deformation. The study was conducted at the temperature range from –100°C to 150°C; the heating rate was 4°C min^{-1}. Thereby the storage modulus (G'), loss modulus (G'') and damping factor (tangent δ) were recorded as a function of temperature. The specimen printing conditions were presented in Table S4.

2.3.4.Melt flow rate (MFR)

A Zwick/Roell load plastometer was used to measure melt flow rate (MFR) and melt volume rate (MVR) of filament before and after printing. The study was conducted according to ISO 1133 standard at the temperature of 200°C and load of 5 kg (n = 5).

2.3.5.Mechanical properties

The parameters provided by the manufacturer of Bioflex® refer to the properties of the solid polymer. Therefore, all the mechanical properties of the filament were studied on printed samples. Furthermore, the influence of raster angle on hardness and tensile properties were investigated, as shown in Table S1. The hardness was measured with a Shore type A durometer (Zwick/Roell, Germany) according to ISO 868 standard. The results are the arithmetic mean of ten measurements. A Zwick/Roell Z020 universal tensile machine was used for tensile testing according to ISO 527 standard. Measurements were carried out at room temperature; crosshead speed was set to 100 mm min^{-1} and initial force was 1 N. Reported results are the average calculated from eight measured dumbbell-shaped specimens. Uniaxial compression test was conducted on solid and porous cubic samples with the dimension of 15 × 15 × 15 mm using a Zwick/Roell Z020 machine. Samples were compressed at a rate of 20 mm min^{-1}

until 50 % strain was reached (n = 5). Detailed information on design and printing conditions were presented in Table S3 and S4.

2.3.6.Surface properties

The contact angle test by the sessile drop technique was applied to determine the wettability and surface free energy (SFE) of Bioflex® printouts. Measurements were performed using ramé-hart 90-U3 goniometer with a DROPimage Pro software (ramé-hart, USA). A 2 µL droplet of selected solvent was deposited on the degreased sample surface and the images were taken. The contact angle was measured for four different solvents, i.e. water, diiodomethane, formamide and ethylene glycol. At least six randomly selected points on the sample surface were tested. In turn, SFE was determined via the Fowkes method in which concept is based on acid-base interactions. Therefore, the contact angle measurements for polar (water) and non-polar (diiodomethane) liquids were used to calculate SFE.

2.4. *In vitro* studies of Bioflex® printed porous structures

2.4.1. Cytotoxicity assay

Cytotoxicity of Bioflex® printouts was studied according to the ISO 10993-5 standard. Firstly, the sample was sterilized 30 min each side under UV radiation. Then, an extract of studies sample was prepared in culturing medium DMEM/F-12 supplemented with FBS; 5 µg ml^{-1} penicillin with streptomycin; 5 µg ml^{-1} amphotericin B (all Coring). The extract thus obtained was incubated for 24 h (37°C, 5% CO_2), filtrated and given to the CCl163 cells which were prepared as follows; cells were seeded on 96-well culture plates with a density of 1000 cells per well (Nunc) and cultured for 24 h (37°C, 5% CO2) in the supplemented DMEM/F-12 culturing medium. After 24 h of cells incubation with extract, the MTT assay was performed. The absorbance of prepared solutions was scanned by Varioskan at λ=570 nm (Thermo Scientific, USA). The results were presented as a cells viability towards control (100% of survival). The statistical analysis was performed with the use of the Origin Pro 8.5 (Washington, DC, USA). Statistical differences were evaluated by the two-way ANOVA (α = 0.05) and post hock Tukey test (α = 0.05).

2.4.2. Degradation studies

The printouts were subjected to an *in vitro* short-term degradation study to estimate degradation susceptibility [26]. Firstly, samples in the shape of disks (□ = 8 mm, h = 3mm) were cut out from the

printed matrix. Then samples were degreased, weighed and placed in 12-well plates. Short-term degradation was conducted for 28 days in strongly alkaline and acidic solutions, 5 M NaOH and 2 M HCl, respectively. 3 ml of selected media was added to each well and incubated at 37°C. Medium was replenished every 2 weeks. After specified time intervals, samples were taken out, rinsed with DI water and dried. The degradation process was monitored by FTIR spectrum and mass measurements. For each time intervals, three replicates were investigated (n = 3).

2.4.3. Bioactivity evaluation in simulated body fluid (SBF)

The *in vitro* bioactivity was tested in an SBF solution prepared according to the procedure developed by Kokubo et al. [24]. Samples for testing were prepared in the same manner as for short-term degradation (n = 3). Incubation was conducted in 6-well plates at 37°C within periods of 7 days, 1 and 3 months. The SBF solution was refreshed every 2 weeks. Incubated samples were removed from the test solution, rinsed with DI water and left to dry at room temperature. The surface morphology of the samples was observed by Scanning Electron Microscope (SEM) (FE-SEM, FEI Quanta FEG 250, accelerating voltage 10 kV) while formed crystals were characterized using EDS and Raman spectroscopy.

3. Results and discussion

3.1. Characterization of chemical structure (ATR-FTIR, Raman)

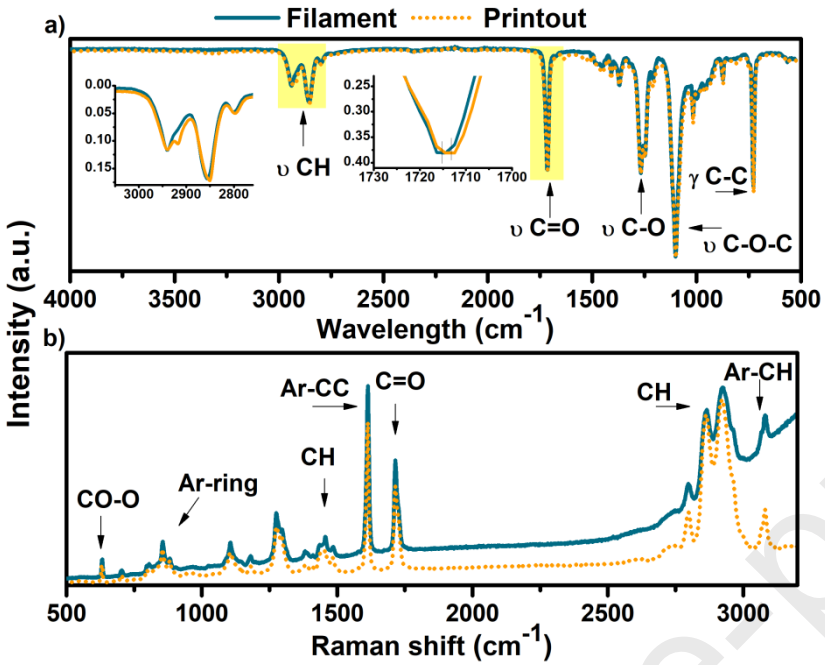

Figure 1 FTIR (a) and Raman (b) spectra of Bioflex® filament and selected printout.

The chemical structure analysis of the filament and printouts was conducted based on FTIR and Raman spectra (Figure 1a,b). According to the information provided by the producer, Bioflex® is a thermoplastic copolyester elastomer (TPC) which suggests the presence of a segmented structure based on a long soft polyester/ether segments (SS) and a short rigid hard segments (HS) [27]. In both samples, absorption peaks at the range of wavenumbers from 3000 to 2795 cm^{-1} indicate the presence of methylene groups. Double peaks at 2929 and 2917 cm^{-1} might be attributed to the stretching vibrations of –CH in the aromatic ring. While signal at 2852 cm^{-1} correspond to the symmetric and asymmetric –CH stretching vibration of aliphatic methylene groups. A slight peak at 2799 cm^{-1} may belong to the methylene group that is adjacent to oxygen. Typical TPCs polyester blocks are represented by the vibration of the carbonyl (C=O) group at ~1713 cm^{-1} and a double absorption peak at 1267 and 1250 cm^{-1} related to the asymmetric and symmetric *v*(C–O) vibration of ester groups. In turn, a sharp band at 1100 cm^{-1} is most likely associated with the presence of the ether oxygen *v*(C–O–C). Bands corresponding to the bending vibrations are visible around 1445 cm^{-1} ($–CH_2$) and ~1015 cm^{-1} (C=O). Strong signal around 724 cm^{-1} correspond to carbon-carbon bonds *γ*(C–C). Additionally, peaks in the range of 1500-1447 cm^{-1} and 874 cm^{-1} might be attributed to the stretching vibration and bending vibration (out of plane) of C=C and –CH of an aromatic ring,

respectively [28–30]. The FTIR spectra of the filament and print are very similar, no significant changes in intensity or band shifts were noted. Nevertheless, analyzing the carbonyl band an upshift of the printout relative to the filament by ~4 cm^{-1} was noted. According to Chen et. al [31], this shift is related to the weakening of hydrogen bonds occurring in the structure. However, the peak is not split thus the presence of H-bonding is rather unlikely or their participation is insignificant. To confirm the above considerations, the Raman spectroscopy was performed. It showed the presence of the following functional groups in the Bioflex® structure; C=O carbonyl groups (single peak at 1714 cm^{-1}); ether oxygen (1104 cm^{-1}), CO-O in-plane deformation of ester groups (632 cm^{-1}); CH_2 deformation vibration at the range of 1434-1488 cm^{-1}; symmetric and asymmetric stretching vibration of –CH (2864, 2924 cm^{-1}). In addition, the Raman spectra confirmed the presence of aromatic rings; Ar–CH stretch at 3065, 3081 cm^{-1}; Ar-CC ring vibration at 1614 cm^{-1}; bending vibration of Ar-ring at the range of 830-880 cm^{-1} [32–35]. In this case, no differences between the filament and printout spectra were observed, also no hydrogen bonded functional groups were found. Thus, it can be concluded that the structure of Bioflex® is based on aromatic polyester-ether compounds connected by ester linkages in which there are no suitable protons that can form H-bonding.

3.2. Thermal properties

Segmented structure of thermoplastic copolyester elastomers (TPC) and their ability to phase separation respond for their dual nature. TPCs act as a crosslinked elastomer at room temperature while after heating they exhibit thermoplastic properties [27]. Bioflex® belongs to TPC group thus to confirm its segmented structure we examined its phase transitions by DSC. Based on the obtained thermograms glass transition temperature (T_g), melting temperature (T_m), heat enthalpy (ΔH_m) and crystallisation temperature (T_c) were determined. The second heating run (Figure 2a) revealed the presence of two melting points at 0.36°C (ΔH_m 14.82 J g^{-1}) and 189.4°C(ΔH_m 4.87 J g^{-1}). The first endothermic transition corresponds to the melting of soft segment crystallites (T_mSS) while the second peak is due to the melting of crystalline hard segments (T_mHS). Relatively low heat enthalpy of T_m(HS) transition could indicate a low crystallinity degree of the hard phase. In turn, the appearance of the T_mSS peak around 0°C points out the presence of relatively long soft segments or/and their high concentration comparing to HS building blocks [36]. The glass transition for both samples occurs around –68.7°C and its slightly higher than the T_g value given in the Bioflex® technical data sheet (–

70°C). This value is associated with the soft phase transition. The T_g of TPCs, which according to the literature reveals at about –70°C, corresponds to the systems based on PTMO (polytetramethylene oxide) soft phase [36–39]. The cooling run (Figure 2b) showed the crystallization temperature of HS at 134.6°C and for SS phase around –30.8°C. The obtained thermograms for the filament and printout overlaps. It can be assumed that the 3D printing process did not cause changes at the microstructure level of Bioflex®.

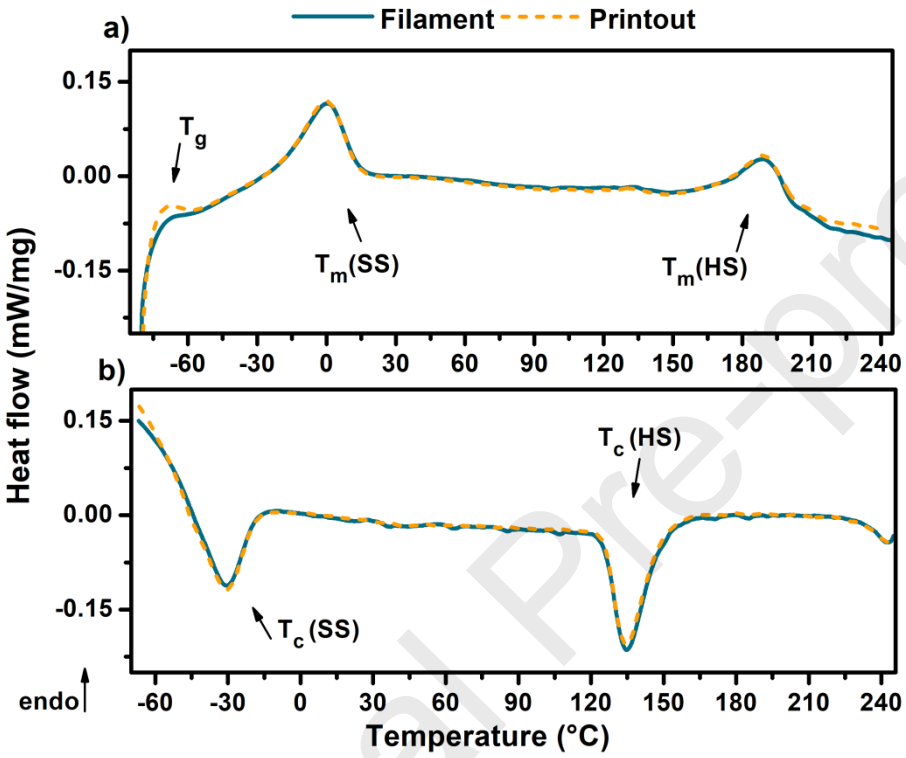

Figure 2 DSC thermograms of filament and Bioflex® printouts. (a) second heating run, (b) cooling run.

TGA measures the amount and rate of change in weight of a sample as temperature function and gives information on its thermal stability. Obtained TG curves and their derivatives are shown in Figure 3. Both thermograms indicate one-step degradation process in the temperature range of 370–470°C. The average thermal stability of filament and printout is around 368°C (T_{onset}). Decomposition process starts at 355°C with a backbone degradation of the material matrix which progresses very rapidly. The printouts exhibited a slightly higher temperature of 90% weight loss and residual mass compared to the filament as given in Table 2. However, such insignificant differences could be due to the little difference in the masses of the tested samples. Thus, conducted thermal studies showed that the Biolex® filament is a thermally stable material that retains its properties after the 3D printing process.

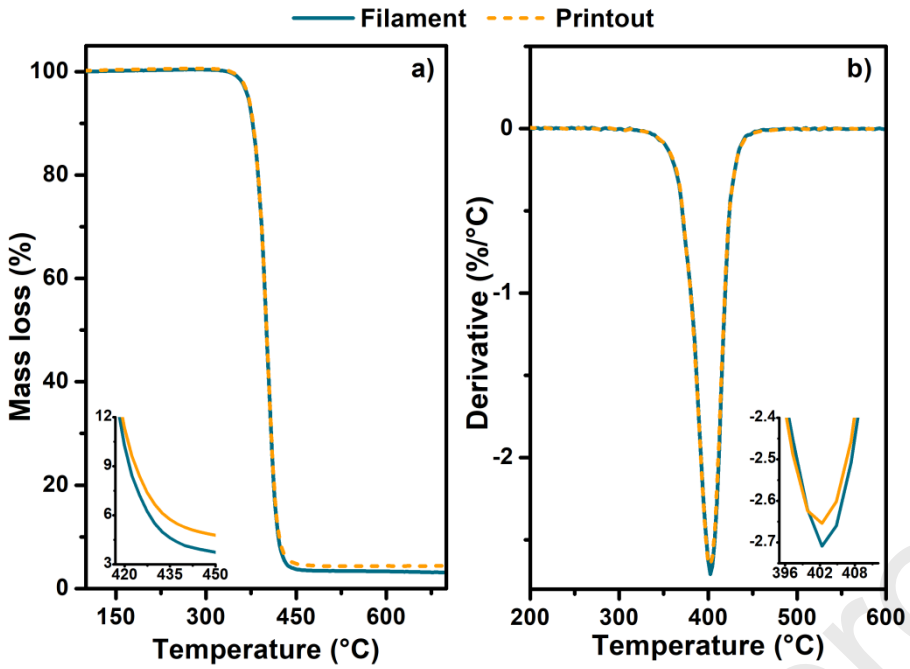

Figure 3 TG (a) and DTG (b) curves for filament and printout of Bioflex®.

	$T_{5\%}$,°C	$T_{10\%}$,°C	$T_{30\%}$,°C	$T_{50\%}$,°C	$T_{90\%}$,°C	Residual mass
Filament	369.8	377.6	392.3	400.7	420.3	3.21% at 697.8°C
Printouts	370.8	378.3	392.4	400.7	421.8	4.37% at 697.9°

Table 2 TGA data: temperature of 5, 10, 30, 50, 90 % weight loss and residual mass.

3.3. Physico-mechanical properties (DMA)

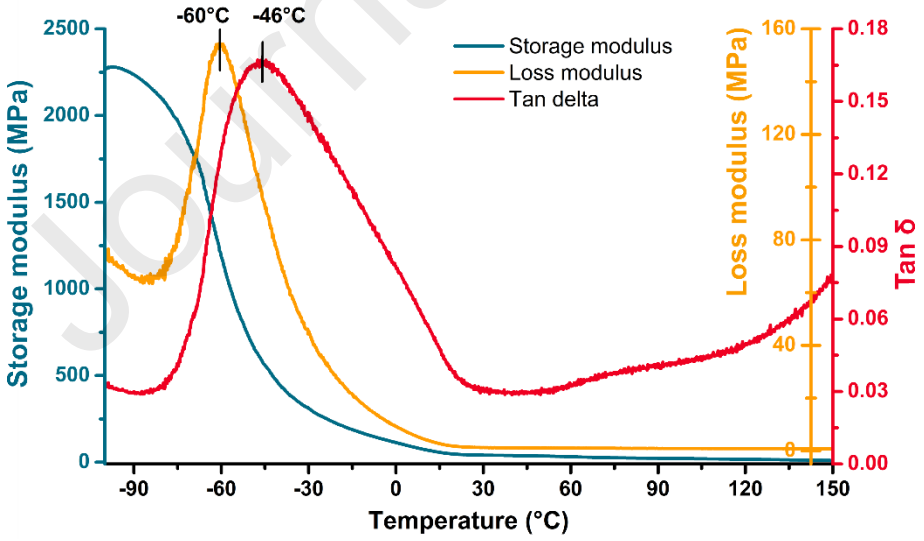

Figure 4 DMA curves of Bioflex® printout - storage, loss modulus and damping parameter.

For further characterization of Bioflex® material, DMA study was performed. DMA can provide additional information on TPC phase behaviour including thermal transitions (T_g, T_m) and mechanical features. For this measurement, a standardized size sample is required thus presented in Figure 4 results refer to printout sample only. Based on the storage modulus curve viscoelastic behaviour regions can be distinguished, a glassy state (at a low-temperature range) with the highest storage modulus value; a glass transition area and region of a rubbery plateau characteristic for thermoplastic elastomers [38]. Tangents delta curve exposes the region of glass transition at the temperature of –75 to 25°C in which the relaxation and transition of soft amorphous phase take place. The maximum of this peak is around –46°C which confirms the presence of PTMO as a soft phase in the structure of Bioflex®, which is consistent with the literature [40]. It is known that amorphous phase in TPCs containing not only the soft segments (e.i PTMO) but it is a mixture of amorphous SS-rich and some noncrystalline hard segments phases [36,40]. Consequently, it can be assumed that a very broad and slight peak around 73°C (Tan δ curve) responds to the T_g of the amorphous HS phase.

The research carried out so far indicates the segmented, hetero-phase structure of the Bioflex® material which belongs to the group of poly(ester ether) copolymers and contains PTMO as a soft segment. Additionally, the filament exhibits outstanding thermal stability and its chemical structure which does not change after the 3D printing process.

3.4. Melt flow rate (MFR)

The melt flow rate (MFR) is an important parameter of thermoplastic materials intended for processing. This parameter represents the rheological properties and is closely associated with a melt viscosity of thermoplastics. FDM/FFF 3DP is based on the extrusion process in which the filament is plasticized in a mini-heating block and deposited on a platform by a heated nozzle with a diameter of 0.15–0.6 mm. Unlike the conventional extrusion process, this operation is devoid of a screw and thus occurring mechanical shear forces are much lower. Therefore, thermoplastic materials for extrusion-based 3DP should be easily plasticized in a relatively short time. Furthermore, such material should be capable of properly solidification (toughening) rate which allows for appropriate interlayer bonding and shape stabilization [41]. The melt rate value is represented as a mass (g, MFR) or volume (cm^3, MVR) of material extruded through the standardized die under constant load and temperature per 10 min. The melt rate of commercial TPC filaments is in the range of MVR = 45 cm^3 10 min^{-1} (Arnitel®,

230°C/2.16 kg), MFR = 28 g 10 min^{-1} (Z-Flex®, 225°C/2.16 kg), MVR = 39 cm^3 10 min^{-1} (FlexiFil®, 230°C/2.16 kg). The data comes from TDS available on the manufacturers' websites.

The results of MFR measurements are presented in Table 3. It was noted that the change in the flow rate of the filament relative to the printout is insignificant. Thus, the printing process did not change the rheological properties of the Bioflex®. Unfortunately, due to the different MFR measurement conditions (temperature/load), these values cannot be directly compared to other commercial products. Is known that as the MFR value increases the print speed of the object can be higher [42]. In turn, to high MFR value might cause uncontrolled leakage of material from the printer nozzle, thereby causing significant defects of the printouts [43].

Table 3 MFR of Bioflex® filament and printouts.

(200°C/5 kg)	MFI (g 10 min^{-1})	MVR (cm^3 10 min^{-1})
Filament	9.14 ± 0.48	9.50 ± 0.50
Printout	9.70 ± 0.63	10.54 ± 0.71

3.5. Mechanical characterization

Table 4 Summary of mechanical tests of printed samples. In the compression test section (P) and (A) mean orientation of cubic specimens during the compression test. P - perpendicular and A- along to plane of the printed layers.

Infill raster orientation	0/90°	±45°
Hardness (Shore A)	76 ± 1	78 ± 1
Young modulus (MPa)	0.16 ± 0.1	0.19 ± 0.1
Tensile strength (MPa)	12.6 ± 1.8	14.1 ± 0.9
Elongation at break (%)	646.7 ± 37.5	757.3 ± 35.7
Relative elongation (%)	318.3 ± 45.2	275.6 ± 42.6
Compression test	Yield point (MPa)	Maximum registered compressive strength (MPa)
Solid_A	0.80 ± 0.12	4.11 ± 0.19
Porous_A	0.61 ± 0.10	2.43 ± 0.15
Solid_P	0.46 ± 0.10	2.54 ± 0.22
Porous_P	0.52 ± 0.11	1.88 ± 0.17

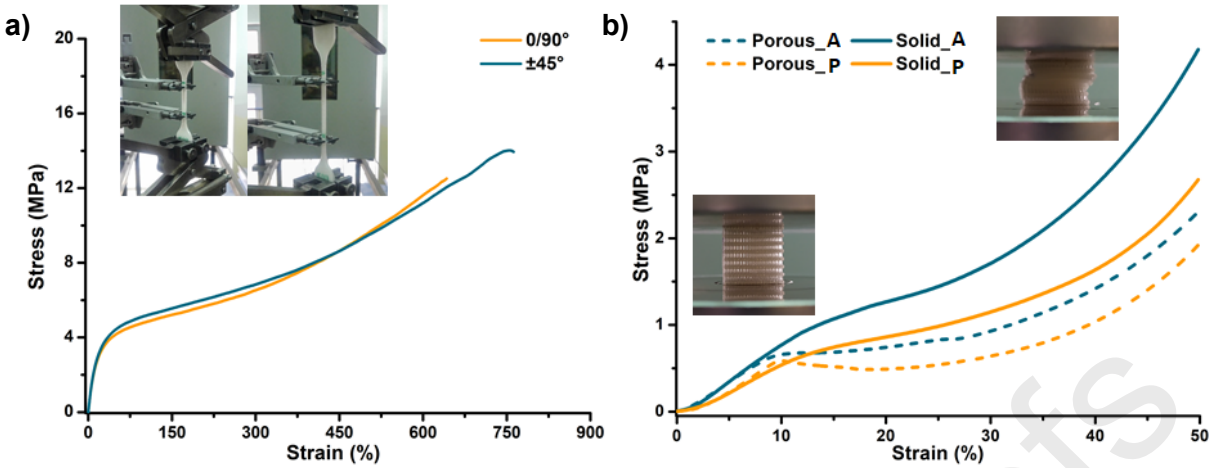

Figure 5 Representative stress-strain curves (a) tensile test (b) compression test.

Further characteristics of the Bioflex® filament included mechanical tests such as hardness, tensile and compression strength. All printing parameters of the test samples were provided in Supplementary data. Several studies have shown that the design and printing parameters significantly affect the printout features [44]. Table 4 presents the results of tensile strength and hardness depending on the applied infill raster orientation as well as compression test data. The hardness of printouts was in the range of 76–78 Sh A, which corresponds to about 22 Sh D. This value is much lower than that given in the Bioflex® TDS (27 ShD) which is probably related to the uneven surface of the printouts formed by successive layers of the oval filament streams. Tensile strength and elongation at break were slightly higher for samples with infill raster orientation ±45° (14 MPa, 760%) than those with raster orientation 0/90°. This is probably due to the higher tension of the layers arranged perpendicular to the stretching direction of the sample [45]. In turn, the tensile strength of raw material from which Bioflex® was formed is 16 MPa thus there is no significant loss of tensile strength after the 3DP process. This may indicate exceptionally good adhesion between successive layers of the printouts. The stress-strain curves (see Figure 5a) of both samples are characteristic of elastomeric materials and their appearance notably resembles curves for TPC with the content of soft segments (SS) exceeding 50 wt% [38].

The compressive strength test was carried out perpendicular (P) and along (A) to the plane of the printed layers (Figure 5b). Solid and porous cubic specimens were tested. Based on the compression curves, three areas distinguished, at low strain narrow elastic region with the yield strength was defined; wide stress plateau where plastic deformation occurs; densification of sample evident by a sharp stress increase. It was noted that the samples tested in the along direction (A) showed markedly

higher values of compressive strength (Table 4). These observations confirm the anisotropic behaviour of the FFF 3D printed samples compared to the solid ones. Similar observations were reported in the Sung-Hoon et al. [46] work, where the compressive strength of ABS samples tested perpendicular to the plane of printed layers was above 20% lower than for specimens tested in the opposite direction. It is worth noting that during the compression test none of the cubic samples was permanently damaged.

3.6. Contact angle (CA) and surface free energy (SFE)

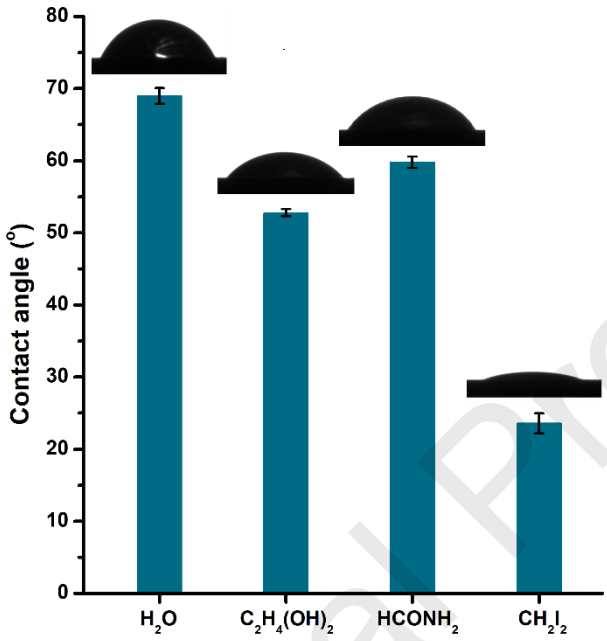

Figure 6 Contact angle of Bioflex® printouts with respect to various liquids.

Contact angle (CA) and surface free energy (SFE) studies provide important information about surface properties, especially when considering Bioflex® as a medical-grade filament. CA results are presented in Figure 6. The water contact angle of 69.0° ± 1.1° indicates a hydrophilic surface with average wettability. Surface free energy was calculated (Fowkes method) using the contact angle against water (polar) and diiodomethane (apolar) liquids. SFE was 52.69 ± 0.16 mN m^{-1} (dispersive part 46.64 ± 0.11 mN m^{-1}, polar part 6.04 ± 0.14 mN m^{-1}). Hydrophilicity (CA around 50-70°) and relatively high surface energy have a beneficial effect on the cells/protein adsorption hence integration between implants and tissues [47,48]. Thus, Bioflex® printouts might be initially considered as elastic implantable products.

3.7. *In vitro* studies of porous structures

This part of the research focuses on *in vitro* studies of an elastic porous matrix printed by using Bioflex® filament to initially examine its potential as a product suitable for short/long-term implantation in the human body. For detail information on printed porous structures, please see Table S3-4 (supplementary data).

3.7.1.Cytotoxicity

The cytotoxicity assay was performed to determine the cytocompatibility of printed structures. The results of cell viability are expressed as the percentage of a control group. The study was performed with the use of established fibroblast cell line CCL-163. Cell viability for all prepared extract concentrations (12.5–100 %) was above 100 % in comparison to the control (Table 5). According to the regulation given in the ISO 10993:5 standard, material which exhibits cell viability higher than 70% (compared to 100% control) can be considered as cytocompatible and non-toxic [49]. Therefore, obtained printouts are qualified as biocompatible. What further confirms that 3D printing process does not cause loss of biocompatibility features relative to the Bioflex® raw material.

Table 5 CCL-163 cells morphology and viability after 24h of contact with extracts obtained by using printed Bioflex®

Extract concentration	100 %	50 %	25 %	12.5 %	control
Cell morphology	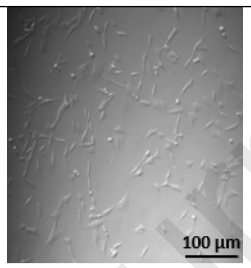	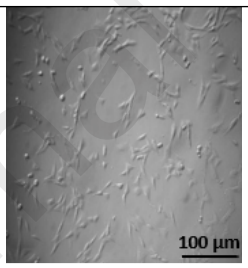	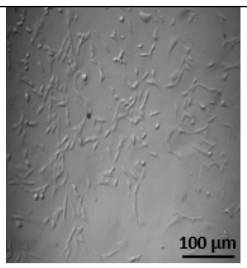	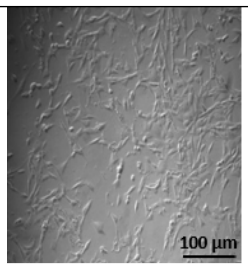	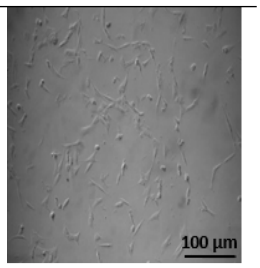
Cell viability (%)	103	108	106	111	100

The morphology of CCL-163 cells was observed after 24h (Table 5). The distribution and shape of cells were comparable to the control. The number of cells markedly increased as the concentration of prepared extract decreased. Nevertheless, Bioflex-exposed cells remain viability even after exposure to 100% extract.

3.7.2.Accelerated degradation studies

One of the method to *in vitro* study degradation susceptibility of polymer materials is so-called accelerated degradation studies. It is a very effective and time-saving method to assess changes

occurring in the material during exposure in environments imitating a human body. High solution concentration allows to markedly reduce the time of examination, which in media such as phosphate-buffered saline (PBS) can last even within a year [21,50].

Accelerated degradation (in 2 M HCl and 5 M NaOH media) included microscopic studies (Table S5), mass loss measurements (Figure 7a) and FTIR examination (Figure 7b) were performed. The results showed that susceptibility to degradation was depended on the solution used. Samples were more sensitive to strongly alkaline medium. After 7 days of incubation, a 3 % mass loss was noted while for the 2M HCl solution mass loss of samples did not exceed 0.5 %. In the acid environment, Bioflex® samples remained practically untouched (mass loss after 28 days around 1.5 %). In turn, in alkaline medium, 10 % weight loss was noticed at the end of the study. The analysis of FTIR spectra confirmed that degradation proceeded primarily as a result of the destruction of the ester bonds present in the Bioflex® structure (Figure 7b). Changes in the peak intensity of ester (νC–O at 1250, 1267 cm^{-1}) and carbonyl (νC=O at 1714 cm^{-1} and δC=O at 1015 cm^{-1}) groups are noticeable in samples incubated in 5M NaOH medium Those minor changes might indicate a significant concentration of resistant to hydrolysis long hydrocarbon chains, i.e. the advantage of high molecular weight soft segments (SS) in the Bioflex® structure.

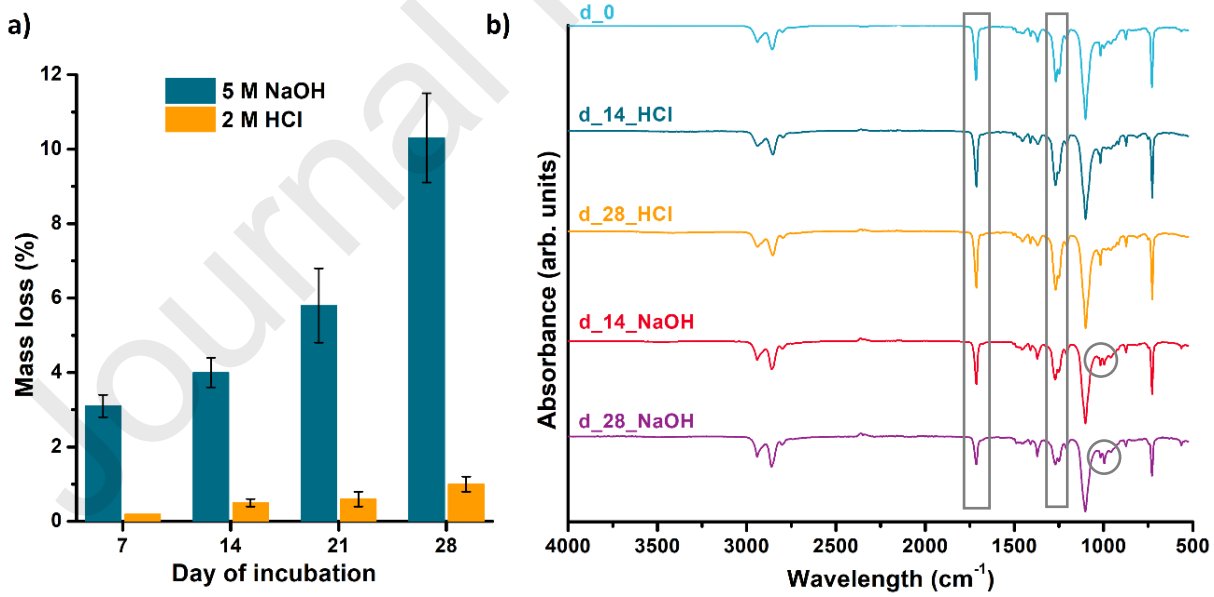

Figure 7 Results of Bioflex® printouts accelerated degradation study performed in 5 M NaOH and 2 M HCl solutions of porous matrix printed using Bioflex® filament, (a) percentage mass loss during degradation, (b) FTIR spectrum collected at a different time of degradation.

PCL is a biodegradable polymer widely used in regenerative medicine application. However, it belongs to the long-term degradable material with the degradation rate event up to 4 years in the

implementation environment. FDM 3D printed porous scaffolds based on PCL during accelerated degradation show a weight loss of 80-90% after about 4 weeks of incubation [21,50]. In turn, polyurethane (TPU) materials dedicated to regenerative purpose in such degradation conditions show a weight loss of 80% (2M HCl) and 20% (5M KOH) after just 15 days of incubation [51]. Thus, the results obtained for porous Bioflex® printouts indicate its high resistance to hydrolysis in such aggressive environments and might be considered as biostable.

This feature may exclude Bioflex® filament for application as degradable tissue-engineered constructs, which should gradually degrade after implantation at the tissue defect site [21,52]. Nonetheless, this does not eliminate the use of this filament for 3D printing of medical equipment, devices and biostable long-term implants representing high resistance to aggressive environments and superb elasticity.

3.7.3.Incubation in simulation body fluid (SBF)

The *in vitro* bioactivity of the printed porous structures was tested in simulated body fluid (SBF) solution over 3 months period. SEM images revealed the crystals deposition on the surface of printouts (Figure 8 a,b). These were observed after 1 month of incubation (Table S6). The crystals presented plate-like morphology, typical for hydroxyapatite (HAp) minerals [53,54], and they were forming agglomerates growing one on another on the printout's surface. The elements of formed crystals were further characterized by EDS measurements (Figure 8 c). EDS analysis revealed the presence of P, Ca, C and O elements which correspond to the chemical formula of HAp ($Ca_{10}(PO_4)_6(OH)_2$). Noticeable signals of carbon and oxygen might also be related to the presence of carbonate in the HAp structure. Trace amounts of magnesium and sodium chloride from the SBF solution have also been noted. The Ca/P atomic ratio was 1.55. It is a lower value than the corresponding to the stoichiometric HAp (Ca/P =1.67), thus formed HAp assumed to be calcium-deficient. It is probably due to the presence of other ions (Mg, Na, CO_3^-) which disturbed the HAp structure. Nevertheless, this dependence is common when biological hydroxyapatite is formed [55].

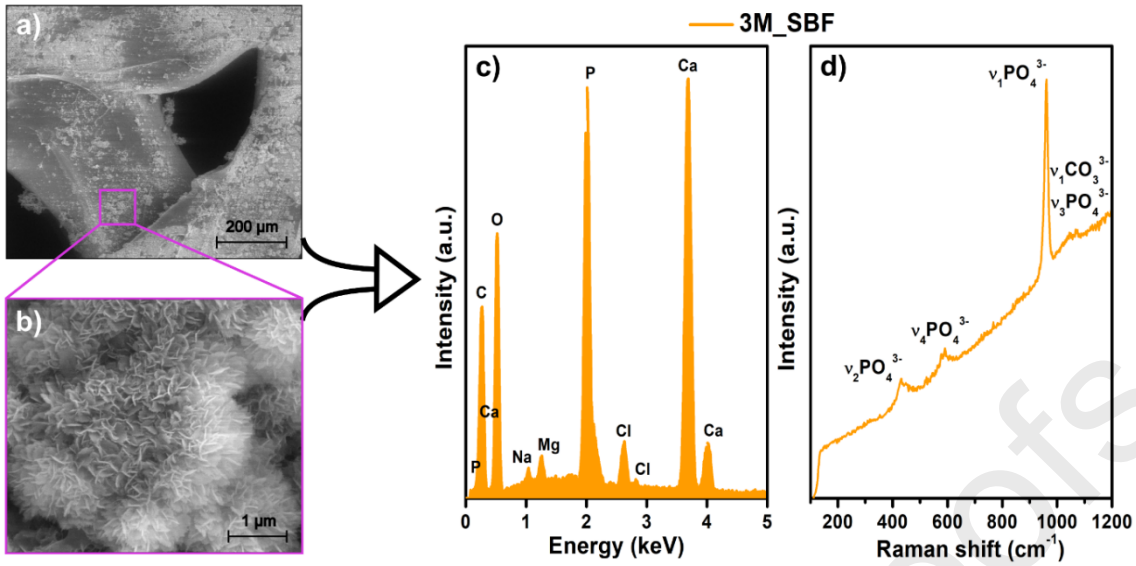

Figure 8 Selected SEM images of Bioflex® printouts after 3 months of incubation in SBF (a,b), and corresponding EDS (c) and Raman (d) spectra of formed crystals. Ca/P ratio is equal to 1.57. SEM images after 1 week and 1 month of incubation can be found in Table S6 (supplementary data).

To support those considerations Raman spectroscopy of deposited crystals was conducted. The spectra show three distinct peaks. The signals at 425 and 588 cm^{-1} correspond to P–O and O–P–O vibrations, respectively. In turn, a sharp peak at 960 cm^{-1} is assigned to stretching vibration of the phosphate group. The presence of a slight signal at the range of 1071 cm^{-1} is attributed to the carbonate groups [56,57]. This explains the registered carbon and oxygen elements in the EDS spectrum. Obtained results indicate the formulation of carbonated-type hydroxyapatites (C-HAp) on the surface of printed structures. According to Kim et al. [54], the existence of carbonate ions in the HAp structure provides enhanced biocompatibility and resorption features compared to synthetic HAp. It has also been shown that such C-HAp is more like natural apatite minerals found in living hard tissues [58].

4. Conclusions

In the presented work, extensive characteristics of the commercial FDM/FFF 3D printing medical-grade filament under the trade name Bioflex® by Filoalfa (Italy) were conducted. Due to the many benefits of using FDM/FFF type 3DP in medicine, there is a need to look for new materials that meet strict medical criteria. The filament market is growing rapidly, however, both in the market and in the literature, attention is mainly devoted to thermoplastic materials such as PLA or PCL and their modifications. Therefore, attention should be paid to materials from the group of thermoplastic elastomers (TPC) that can fill the gap of high-flexibility medical filaments.

Partial conclusions in the study are as follows:

1. Performed spectroscopic, thermal, thermomechanical and rheological analysis showed that 3D printing does not cause changes in the filament structure. No signs of degradation or changes in thermal properties of resulted printouts were noted. Thus, the Bioflex® filament is highly stable under 3D printing conditions.
2. Based on the performed studies and literature overview it was found out that Bioflex® belongs to the thermoplastic copolyester-ether elastomer (TPC) polymer group with the polythtramethylne oxide (PTMO) as a soft segment (SS). The results of thermal studies, hardness and tensile stress-strain curves also suggest that it is a material with an advantage of SS phase in the structure.
3. It has been observed that the infill orientation and build orientation affects the mechanical properties of printouts.
4. Contact angle study revealed hydrophilic properties of Bioflex® printouts surface.
5. *In vitro* cytotoxicity studies confirmed that the Bioflex® printouts meet the criteria of biocompatibility, according to the ISO 10993:5 standard.
6. Accelerated degradation studies showed outstanding resistance to hydrolysis of Bioflex® printouts which exclude its application as degradable medical constructs.
7. Incubation of Bioflex® printouts in SBF solution revealed deposition of carbonate hydroxyapatite (C-HAp) at their surface. Therefore, its application can be considered in the field of bone or cartilage engineering.

In this article, we wanted to pay attention of filament manufacturers to provide extended material characterization in their technical datasheet. In the case of this study, Bioflex® occurred to be suitable for FDM/FFF 3DP of medical equipment, devices and internal long-term implants. This is due to its sufficient biocompatibility and outstanding resistance to hydrolysis and aggressive environments. With all of the data provided in this article further development of FDM/FFF 3DP with the use of Bioflex® will be continued. In summary, this work provides relevant information in both material and application as well as creates a strong basis for further more advanced biological and medical researches.

CRediT authorship contribution statement

Agnieszka Haryńska: Conceptualization, Methodology, Software, Validation, Investigation, Writing - Original Draft, Writing - Review & Editing, Visualization, Project administration. **Iga Carayon:** Formal analysis, Investigation, Resources, Writing - Review & Editing. **Paulina Kosmela:** Investigation. **Kamil Szeliski:** Investigation. **Marcin Łapiński:** Investigation. **Marta Pokrywczyńska:** Investigation. **Justyna Kucińska-Lipka**: Resources, Writing - Review & Editing. **Helena Janik**: Resources, Writing - Review & Editing.

Acknowledgements

We acknowledge MSc Dawid Zakrzewski for conducting tensile strength test.

Conflicts of interest

The authors declare no conflict of interest.

Appendix. Supplementary material

Supplementary data

Data availability

The raw/processed data required to reproduce these findings cannot be shared at this time due to technical or time limitations. However, they may be made available on request.

References

[1] A.J.T. Teo, A. Mishra, I. Park, Y.J. Kim, W.T. Park, Y.J. Yoon, Polymeric Biomaterials for Medical Implants and Devices, ACS Biomater. Sci. Eng. 2 (2016) 454–472. https://doi.org/10.1021/acsbiomaterials.5b00429.

[2] A. Aimar, A. Palermo, B. Innocenti, The Role of 3D Printing in Medical Applications: A State of the Art, J. Healthc. Eng. (2019). https://doi.org/10.1155/2019/5340616.

[3] C. Lee Ventola, Medical applications for 3D printing: Current and projected uses, Pharm. Ther. 39 (2014) 704–711.

[4] Afsana, V. Jain, N. Haider, K. Jain, 3D Printing in Personalized Drug Delivery, Curr. Pharm. Des. 24 (2019) 5062–5071. https://doi.org/10.2174/1381612825666190215122208.

[5] J. Garcia, Z. Yang, R. Mongrain, R.L. Leask, K. Lachapelle, 3D printing materials and their use in medical education: a review of current technology and trends for the future, BMJ Simul. Technol. Enhanc. Learn. (2017) bmjstel-2017-000234. https://doi.org/10.1136/bmjstel-2017-000234.

[6] F. Govsa, T. Yagdi, M.A. Ozer, C. Eraslan, A.K. Alagoz, Building 3D anatomical model of coiling of the internal carotid artery derived from CT angiographic data, Eur. Arch. Oto-Rhino-Laryngology. 274 (2017) 1097–1102. https://doi.org/10.1007/s00405-016-4355-0.

[7] M. Chung, N. Radacsi, C. Robert, E.D. McCarthy, A. Callanan, N. Conlisk, P.R. Hoskins, V. Koutsos, On the optimization of low-cost FDM 3D printers for accurate replication of patient-

specific abdominal aortic aneurysm geometry, 3D Print. Med. 4 (2018) 2. https://doi.org/10.1186/s41205-017-0023-2.

[8] M.C. Luque, A. Calleja-Hortelano, P.E. Romero, Use of 3D printing in model manufacturing for minor surgery training of general practitioners in primary care, Appl. Sci. 9 (2019). https://doi.org/10.3390/app9235212.

[9] G. Verstraete, A. Samaro, W. Grymonpré, V. Vanhoorne, B. Van Snick, M.N. Boone, T. Hellemans, L. Van Hoorebeke, J.P. Remon, C. Vervaet, 3D printing of high drug loaded dosage forms using thermoplastic polyurethanes, Int. J. Pharm. 536 (2018) 318–325. https://doi.org/10.1016/j.ijpharm.2017.12.002.

[10] T.C. Okwuosa, C. Soares, V. Gollwitzer, R. Habashy, P. Timmins, M.A. Alhnan, On demand manufacturing of patient-specific liquid capsules via co-ordinated 3D printing and liquid dispensing, Eur. J. Pharm. Sci. 118 (2018) 134–143. https://doi.org/10.1016/j.ejps.2018.03.010.

[11] A. Goyanes, A.B.M. Buanz, A.W. Basit, S. Gaisford, Fused-filament 3D printing (3DP) for fabrication of tablets, Int. J. Pharm. 476 (2014) 88–92. https://doi.org/10.1016/j.ijpharm.2014.09.044.

[12] J.A. Weisman, D.H. Ballard, U. Jammalamadaka, K. Tappa, J. Sumerel, H.B. D'Agostino, D.K. Mills, P.K. Woodard, 3D Printed Antibiotic and Chemotherapeutic Eluting Catheters for Potential Use in Interventional Radiology: In Vitro Proof of Concept Study, Acad. Radiol. 26 (2019) 270–274. https://doi.org/10.1016/j.acra.2018.03.022.

[13] E. Mathew, J. Domínguez-Robles, S.A. Stewart, E. Mancuso, K. O'Donnell, E. Larrañeta, D.A. Lamprou, Fused Deposition Modeling as an Effective Tool for Anti-Infective Dialysis Catheter Fabrication, ACS Biomater. Sci. Eng. 5 (2019) 6300–6310. https://doi.org/10.1021/acsbiomaterials.9b01185.

[14] A.L. Tyson, S.T. Hilton, L.C. Andreae, Rapid, simple and inexpensive production of custom 3D printed equipment for large-volume fluorescence microscopy, Int. J. Pharm. 494 (2015) 651–656. https://doi.org/10.1016/j.ijpharm.2015.03.042.

[15] G.I.J. Salentijn, P.E. Oomen, M. Grajewski, E. Verpoorte, Fused Deposition Modeling 3D Printing for (Bio)analytical Device Fabrication: Procedures, Materials, and Applications, Anal. Chem. 89 (2017) 7053–7061. https://doi.org/10.1021/acs.analchem.7b00828.

[16] I. Buj-Corral, A. Bagheri, O. Petit-Rojo, 3D Printing of Porous Scaffolds with Controlled Porosity and Pore Size Values, Materials (Basel). 11 (2018) 1532. https://doi.org/10.3390/ma11091532.

[17] C. Esposito Corcione, F. Gervaso, F. Scalera, S.K. Padmanabhan, M. Madaghiele, F. Montagna, A. Sannino, A. Licciulli, A. Maffezzoli, Highly loaded hydroxyapatite microsphere/ PLA porous scaffolds obtained by fused deposition modelling, Ceram. Int. 45 (2019) 2803–2810. https://doi.org/10.1016/j.ceramint.2018.07.297.

[18] S. Chen, L. Zhu, W. Wen, L. Lu, C. Zhou, B. Luo, Fabrication and Evaluation of 3D Printed Poly(l -lactide) Scaffold Functionalized with Quercetin-Polydopamine for Bone Tissue Engineering, ACS Biomater. Sci. Eng. 5 (2019) 2506–2518. https://doi.org/10.1021/acsbiomaterials.9b00254.

[19] C. Capone, L. Di Landro, F. Inzoli, M. Penco, L. Sartore, Thermal and Mechanical Degradation During Polymer Extrusion Processing, Polym. Eng. Sci. 47 (2007) 1813–1819. https://doi.org/10.1002/pen.20882.

[20] G.D. Goh, Y.L. Yap, H.K.J. Tan, S.L. Sing, G.L. Goh, W.Y. Yeong, Process–Structure–Properties in Polymer Additive Manufacturing via Material Extrusion: A Review, Crit. Rev. Solid State Mater. Sci. 45 (2020) 113–133. https://doi.org/10.1080/10408436.2018.1549977.

[21] M. Mohseni, D.W. Hutmacher, N.J. Castro, Independent evaluation of medical-grade bioresorbable filaments for fused deposition modelling/fused filament fabrication of tissue engineered constructs, Polymers (Basel). 10 (2018). https://doi.org/10.3390/polym10010040.

[22] C.G. Liu, Y.T. Zeng, R.K. Kankala, S.S. Zhang, A.Z. Chen, S. Bin Wang, Characterization and

preliminary biological evaluation of 3D-printed porous scaffolds for engineering bone tissues, Materials (Basel). 11 (2018). https://doi.org/10.3390/ma11101832.

[23] D.W. Hutmacher, T. Schantz, I. Zein, K.W. Ng, S.H. Teoh, K.C. Tan, Mechanical properties and cell cultural response of polycaprolactone scaffolds designed and fabricated via fused deposition modeling, J. Biomed. Mater. Res. 55 (2001) 203–216. https://doi.org/10.1002/1097-4636(200105)55:2<203::AID-JBM1007>3.0.CO;2-7.

[24] T. Kokubo, H. Takadama, How useful is SBF in predicting in vivo bone bioactivity?, Biomaterials. 27 (2006) 2907–2915. https://doi.org/10.1016/j.biomaterials.2006.01.017.

[25] T. Kokubo, H. Takadama, Simulated Body Fluid (SBF) as a Standard Tool to Test the Bioactivity of Implants, in: Handb. Biominer., Wiley-VCH Verlag GmbH, Weinheim, Germany, 2008: pp. 97–109. https://doi.org/10.1002/9783527619443.ch51.

[26] S.M. Cetina-Diaz, L.H. Chan-Chan, R.F. Vargas-Coronado, J.M. Cervantes-Uc, P. Quintana-Owen, K. Paakinaho, M. Kellomaki, L. Di Silvio, S. Deb, J. V. Cauich-Rodríguez, Physicochemical characterization of segmented polyurethanes prepared with glutamine or ascorbic acid as chain extenders and their hydroxyapatite composites, J. Mater. Chem. B. 2 (2014) 1966–1976. https://doi.org/10.1039/c3tb21500h.

[27] J. Djonlagic, M.S. Nikolic, Thermoplastic Copolyester Elastomers, in: Handb. Eng. Spec. Thermoplast. Polyethers Polyesters, John Wiley and Sons, Hoboken, NJ, USA, 2011: pp. 377–427. https://doi.org/10.1002/9781118104729.ch10.

[28] G. Socrates, Infrared and Raman Characteristic Group Frequencies: Tables and Charts, third, John Wiley & Sons, Ltd., 2004. https://doi.org/10.1002/jrs.1238.

[29] Y. Davies, J. Davies, M.J. Forrest, Infrared Spectra of Rubbers, Plastics and Thermoplastic Elastomers, De Gruyter, Berlin, Boston, 2019. https://doi.org/10.1515/9783110645750.

[30] V. Nagarajan, A.K. Mohanty, M. Misra, Blends of polylactic acid with thermoplastic copolyester elastomer: Effect of functionalized terpolymer type on reactive toughening, Polym. Eng. Sci. 58 (2018) 280–290. https://doi.org/10.1002/pen.24566.

[31] J. Chen, Q. Lv, D. Wu, X. Yao, J. Wang, Z. Li, Nucleation of a Thermoplastic Polyester Elastomer Controlled by Silica Nanoparticles, Ind. Eng. Chem. Res. 55 (2016) 5279–5286. https://doi.org/10.1021/acs.iecr.5b04464.

[32] E. Rebollar, S. Pérez, M. Hernández, C. Domingo, M. Martín, T.A. Ezquerra, J.P. García-Ruiz, M. Castillejo, *P*hysicochemical modifications accompanying UV laser induced surface structures on poly(ethylene terephthalate) and their effect on adhesion of mesenchymal cells, Phys. Chem. Chem. Phys. 16 (2014) 17551–17559. https://doi.org/10.1039/c4cp02434f.

[33] S. Betelu, I. Tijunelyte, L. Boubekeur-Lecaque, I. Ignatiadis, A. Schnepf, E. Guenin, N. Bouchemal, N. Felidj, E. Rinnert, M. Lamy de la Chapelle, Raman Characterization of Phenyl-Derivatives: From Primary Amine to Diazonium Salts, J. Org. Inorg. Chem. 3 (2017) 1–10. https://doi.org/10.21767/2472-1123.100021.

[34] J. James, G. V. Thomas, K. Pramoda, N. Kalarikkal, S. Thomas, Thermoplastic-elastomer composition based on an interpenetrating polymeric network of styrene butadiene rubber-poly(methyl methacrylate) as an efficient vibrational damper, New J. Chem. 42 (2018) 1939–1951. https://doi.org/10.1039/c7nj03998k.

[35] F. Adar, Introduction to Interpretation of Raman Spectra Using Database Searching and Functional Group Detection and Identification, Spectroscopy. 31 (2016) 16–23.

[36] W. Gabriëlse, M. Soliman, K. Dijkstra, Microstructure and phase behavior of block copoly(ether ester) thermoplastic elastomers, Macromolecules. 34 (2001) 1685–1693. https://doi.org/10.1021/ma0012696.

[37] J. Krijgsman, D. Husken, R.J. Gaymans, Synthesis and properties of thermoplastic elastomers based on PTMO and tetra-amide, Polymer (Guildf). 44 (2003) 7573–7588. https://doi.org/10.1016/j.polymer.2003.09.043.

[38] A. Szymczyk, E. Senderek, J. Nastalczyk, Z. Roslaniec, New multiblock poly(ether-ester)s based on poly(trimethylene terephthalate) as rigid segments, Eur. Polym. J. 44 (2008) 436–443. https://doi.org/10.1016/j.eurpolymj.2007.11.005.

[39] S. Paszkiewicz, A. Szymczyk, Z. Špitalský, J. Mosnáček, K. Kwiatkowski, Z. Rosłaniec, Structure and properties of nanocomposites based on PTT-block-PTMO copolymer and graphene oxide prepared by in situ polymerization, Eur. Polym. J. 50 (2014) 69–77. https://doi.org/10.1016/j.eurpolymj.2013.10.031.

[40] R.J. Zhou, T. Burkhart, Thermal and mechanical properties of poly(ether ester)-based thermoplastic elastomer composites filled with TiO2 nanoparticles, J. Mater. Sci. 46 (2011) 2281–2287. https://doi.org/10.1007/s10853-010-5068-1.

[41] J. Yin, C. Lu, J. Fu, Y. Huang, Y. Zheng, Interfacial bonding during multi-material fused deposition modeling (FDM) process due to inter-molecular diffusion, Mater. Des. 150 (2018) 104–112. https://doi.org/10.1016/j.matdes.2018.04.029.

[42] M.H. Khaliq, R. Gomes, C. Fernandes, J. Nóbrega, O.S. Carneiro, L.L. Ferrás, On the use of high viscosity polymers in the fused filament fabrication process, Rapid Prototyp. J. 23 (2017) 727–735. https://doi.org/10.1108/RPJ-02-2016-0027.

[43] D. Hua, X. Zhang, Z. Ji, C. Yan, B. Yu, Y. Li, X. Wang, F. Zhou, 3D printing of shape changing composites for constructing flexible paper-based photothermal bilayer actuators, J. Mater. Chem. C. 6 (2018) 2123–2131. https://doi.org/10.1039/c7tc05710e.

[44] D. Popescu, A. Zapciu, C. Amza, F. Baciu, R. Marinescu, FDM process parameters influence over the mechanical properties of polymer specimens: A review, Polym. Test. 69 (2018) 157–166. https://doi.org/10.1016/j.polymertesting.2018.05.020.

[45] A.K. Sood, R.K. Ohdar, S.S. Mahapatra, Parametric appraisal of mechanical property of fused deposition modelling processed parts, Mater. Des. 31 (2010) 287–295. https://doi.org/10.1016/j.matdes.2009.06.016.

[46] S.H. Ahn, M. Montero, D. Odell, S. Roundy, P.K. Wright, Anisotropic material properties of fused deposition modeling ABS, 2002. https://doi.org/10.1108/13552540210441166.

[47] M.M. Gentleman, E. Gentleman, The role of surface free energy in osteoblast-biomaterial interactions, Int. Mater. Rev. 59 (2014) 417–429. https://doi.org/10.1179/1743280414Y.0000000038.

[48] S.H. Kim, H.J. Ha, Y.K. Ko, S.J. Yoon, J.M. Rhee, M.S. Kim, H.B. Lee, G. Khang, Correlation of proliferation, morphology and biological responses of fibroblasts on LDPE with different surface wettability, J. Biomater. Sci. Polym. Ed. 18 (2007) 609–622. https://doi.org/10.1163/156856207780852514.

[49] ISO/EN10993-5, Biological Evaluation of Medical Devices—Part 5: Tests for in Vitro Cytotoxicity, 3rd ed., Int. Organ. Stand. Geneva, Switz. (2009).

[50] C.X.F. Lam, M.M. Savalani, S.H. Teoh, D.W. Hutmacher, Dynamics of in vitro polymer degradation of polycaprolactone-based scaffolds: Accelerated versus simulated physiological conditions, Biomed. Mater. 3 (2008). https://doi.org/10.1088/1748-6041/3/3/034108.

[51] I. Gubanska, J. Kucinska-Lipka, H. Janik, The influence of amorphous macrodiol, diisocyanate type and L-ascorbic acid modifier on chemical structure, morphology and degradation behavior of polyurethanes for tissue scaffolds fabrication, Polym. Degrad. Stab. 163 (2019) 52–67. https://doi.org/10.1016/j.polymdegradstab.2019.02.025.

[52] J. Kucińska-Lipka, I. Gubanska, A. Skwarska, Microporous polyurethane thin layer as a promising scaffold for tissue engineering, Polymers (Basel). 9 (2017). https://doi.org/10.3390/polym9070277.

[53] Z. Gou, J. Chang, J. Gao, Z. Wang, In vitro bioactivity and dissolution of Ca2(SiO3)(OH)2 and β-Ca2SiO4 fibers, J. Eur. Ceram. Soc. 24 (2004) 3491–3497. https://doi.org/10.1016/j.jeurceramsoc.2003.11.023.

[54] S. Kim, C.B. Park, Mussel-inspired transformation of CaCO3 to bone minerals, Biomaterials. 31 (2010) 6628–6634. https://doi.org/10.1016/j.biomaterials.2010.05.004.

[55] B. Wopenka, J.D. Pasteris, A mineralogical perspective on the apatite in bone, in: Mater. Sci. Eng. C, Elsevier, 2005: pp. 131–143. https://doi.org/10.1016/j.msec.2005.01.008.

[56] A. Awonusi, M.D. Morris, M.M.J. Tecklenburg, Carbonate assignment and calibration in the Raman spectrum of apatite, Calcif. Tissue Int. 81 (2007) 46–52. https://doi.org/10.1007/s00223-007-9034-0.

[57] D. Bellucci, G. Bolelli, V. Cannillo, A. Cattini, A. Sola, In situ Raman spectroscopy investigation of bioactive glass reactivity: Simulated body fluid solution vs TRIS-buffered solution, Mater. Charact. 62 (2011) 1021–1028. https://doi.org/10.1016/j.matchar.2011.07.008.

[58] E. Landi, G. Celotti, G. Logroscino, A. Tampieri, Carbonated hydroxyapatite as bone substitute, J. Eur. Ceram. Soc. 23 (2003) 2931–2937. https://doi.org/10.1016/S0955-2219(03)00304-2.

A COMPREHENSIVE EVALUATION OF FLEXIBLE FDM/FFF 3D PRINTING FILAMENT AS A POTENTIAL MATERIAL IN MEDICAL APPLICATION

Agnieszka Haryńska[1,*], Iga Carayon[1], Paulina Kosmela[1], Kamil Szeliski[3], Marcin Łapiński[2], Marta Pokrywczyńska[3], Justyna Kucińska-Lipka[1], Helena Janik[1]

[1] Department of Polymers Technology, Faculty of Chemistry, Gdansk University of Technology (GUT), Narutowicza Street 11/12, 80-233 Gdansk, Poland

[2] Department of Solid State Physics, Faculty of Applied Physics and Mathematics, Gdansk University of Technology (GUT), Narutowicza Street 11/12, 80-233 Gdansk, Poland

[3] Department of Regenerative Medicine, Cell and Tissue Bank, Nicolaus Copernicus University, Collegium Medicum, M.Sklodowskiej-Curie 9, 85-094 Bydgoszcz, Poland

* Correspondence: agnieszka.harynska@pg.edu.pl (AH)

CRediT authorship contribution statement

Agnieszka Haryńska: Conceptualization, Methodology, Software, Validation, Investigation, Writing - Original Draft, Writing - Review & Editing, Visualization, Project administration. **Iga Carayon:** Formal analysis, Investigation, Resources, Writing - Review & Editing. **Paulina Kosmela:** Investigation. **Kamil Szeliski:** Investigation. **Marcin Łapiński:** Investigation. **Marta Pokrywczyńska:** Investigation. **Justyna Kucińska-Lipka**: Resources, Writing - Review & Editing. **Helena Janik**: Resources, Writing - Review & Editing.

Declaration of interests

☒ The authors declare that they have no known competing financial interests or personal relationships that could have appeared to influence the work reported in this paper.

☐The authors declare the following financial interests/personal relationships which may be considered as potential competing interests:

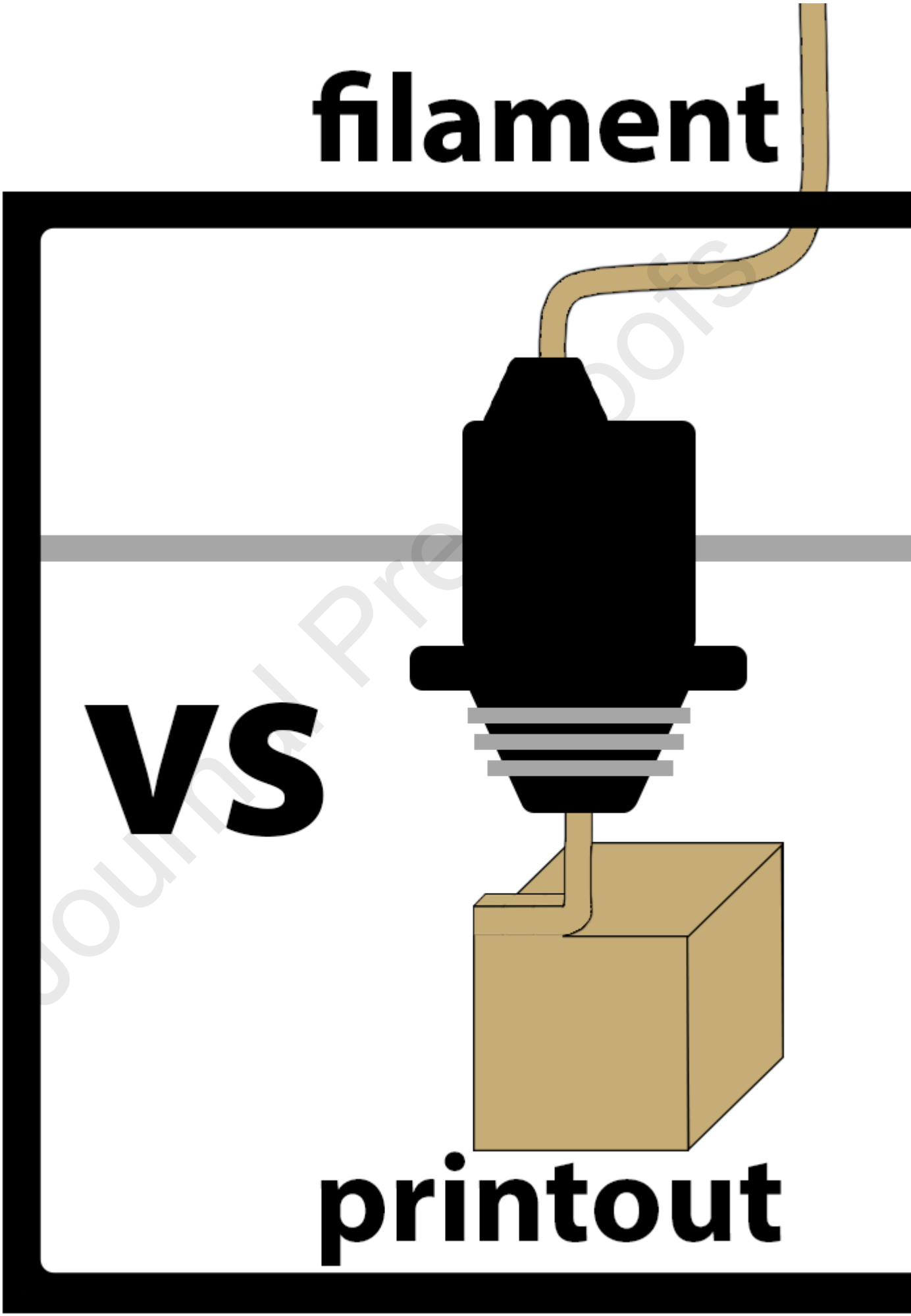

Highlights

- Medical grade flexible filament for FDM 3DP was studied.
- The effects of FDM 3D printing process on filament were studied.
- Physical, chemical, mechanical, surface and thermal properties of filament and printouts were characterized.
- FDM 3DP process does not change the filament structure and properties.
- A series of *in vitro* studies have shown that formed printouts have great potential for use in FDM 3DP of medical devices and internal long-term cartilage or bone implants.